International Journal of Multiphase Flow 34 (2008) 1119–1129

Contents lists available at ScienceDirect

International Journal of Multiphase Flow

journal homepage: www.elsevier.com/locate/ijmulflow

The hydrodynamics of liquid–liquid upflow through a venturimeter

Arun Kumar Jana [a,b], Gargi Das [a,*], Prasanta Kumar Das [c]

[a] Department of Chemical Engineering, Indian Institute of Technology, Kharagpur 721 302, West Bengal, India
[b] Department of Chemical Engineering, S.V. National Institute of Technology, Surat 395 007, Gujarat, India
[c] Department of Mechanical Engineering, Indian Institute of Technology, Kharagpur 721 302, West Bengal, India

ARTICLE INFO

Article history:
Received 20 June 2008
Received in revised form 26 June 2008
Accepted 26 June 2008
Available online 18 July 2008

ABSTRACT

The present work reports the influence of a venturimeter on liquid–liquid phase distribution during upflow through a vertical pipe. The optical probe technique has been adopted for the characterization of flow. The probability density function and the wavelet multi-resolution analysis of the random probe signals have provided an insight into the details of the flow patterns and the intrinsic differences at the upstream, throat and the downstream sections. The experiments have indicated the flow pattern transitions to occur at lower velocities at the downstream region of the venturi. The pressure drop readings across the venturi have been used to estimate the mass flow rate of the mixture by using suitable models for the different patterns.

1. Introduction

Oil–water two-phase flow commonly occurs in well-bores, subsea pipelines, extraction equipment, etc. During the cocurrent flow of oil–water mixtures through conduits, the fluids distribute themselves into different interfacial configurations which are termed as flow patterns or flow regimes. The hydrodynamics of two-phase flow strongly depends on the existing flow patterns. There have been several studies on the hydrodynamics of oil–water two-phase flow through horizontal (Russell et al., 1959; Charles et al., 1961; Guzhov et al., 1973; Valle and Kvandal, 1995; Trallero, 1995; Angeli and Hewitt, 2000; Chakrabarti et al., 2007) and vertical (Govier et al., 1961; Brown and Govier, 1961; Farrar and Bruun, 1996; Jana et al., 2006a,b) conduits. This includes estimation of flow patterns by adopting various measurement techniques (Jana et al., 2007), study of holdup and pressure drop (Angeli and Hewitt, 1998; Chakrabarti et al., 2007) in the different flow patterns, etc. Some studies (Lovick and Angeli, 2004; Ioannou et al., 2004, 2005; Chakrabarti et al., 2006; Hu and Angeli, 2006) have also been performed to understand phase inversion in flow systems. The theoretical studies (Yeh et al., 1964; Brauner, 2001; Brauner and Ullmann, 2002; Ullmann and Brauner, 2006) on liquid–liquid flows have attempted to predict flow pattern boundaries and phase inversion. Most of the above studies report liquid–liquid flow through channels of uniform cross-section. A change in cross-section can influence the phase distribution of a two-phase mixture both in the upstream and downstream regions. However, this aspect has rarely been investigated in liquid–liquid two-phase flows. Further, online metering of two-phase flow is an open technical challenge.

Oddie and Pearson (2004) have described several online, continuous flow measurement techniques for gas–liquid, gas–solid, liquid–solid, and liquid–liquid systems. This includes venturi pressure drop, Coriolis, electromagnetic, and cross-correlation flow meters, γ-ray absorption and gradio-manometer densitometry, as well as local electrical and fiber-optic sensors. Pal (1993) has investigated the applicability of conventional orifice and venturi meters to monitor the flow rate of oil–water emulsions and concluded that the orifice and venturi calibration curves (discharge coefficient versus Reynolds number) obtained from any single-phase Newtonian fluid are applicable to surfactant-stabilized emulsions.

Thang and Davis (1979) investigated the phase structure during vertical bubbly flow of air–water mixture through venturies. The authors have adopted the resistivity probe technique to measure local void fraction, bubble velocity, bubble detection rate and probability density distribution of bubble sizes in the flow. They observed bubble coalescence in the converging section and bubble fragmentation in the diverging section. Thang and Davis (1981) investigated pressure distribution during air-water flow. They developed an analysis to predict the pressure rise across a shock wave and compared the static pressure measurements obtained in eight venturi assemblies with theoretical prediction.

Several theoretical studies (Boyer and Lemonnier, 1996; Werven et al., 2003; Rosa and Morales, 2004) and experimental researches (Silva et al., 1991; Rosa and Morales, 2004; Steven, 2002; Zhang et al., 2005) have been carried out and a number of correlations have been proposed to estimate gas–liquid flow from pressure drop measurements across a venturimeter. The studies include air–water flows (Soubiran and Sherwood, 2000; Gaston and Reizes, 2001), oil–gas flows (Zhang et al., 2005; Huang et al.,

* Corresponding author. Tel.: +91 3222 283952; fax: +91 3222 255303.
E-mail address: gargi@che.iitkgp.ernet.in (G. Das).

0301-9322/$ - see front matter © 2008 Elsevier Ltd. All rights reserved.
doi:10.1016/j.ijmultiphaseflow.2008.06.008

2005) and wet gas metering (Steven, 2002; Xu et al., 2003). Most of the researchers (Zhang et al., 2005; Huang et al., 2005) have used a flow pattern detector or void fraction meter in addition to a venturimeter for measurement of the total flow rate. There have also been some attempts (Katheder and Susser, 1989; Huang and Sciver, 1996) to predict the flow rate of two-phase helium flow.

Liquid–liquid flow through a venturi section incorporated in a vertical pipeline is investigated in the present study. The motivation of the present study is twofold. Development of flow phenomena through a convergent–divergent section has been studied. Efforts have also been made to study the performance of a venturimeter as a two-phase mass flow meter for liquid–liquid flows.

2. Experimental setup and procedure

The schematic diagram of the setup is shown in Fig. 1. It consists of a test rig and accessories namely water tank, kerosene tank, kerosene–water separator, two centrifugal pumps and measuring equipment. The test rig comprises of a vertical transparent acrylic resin tube of 0.0254 m diameter and 4 m length. Acrylic resin is selected as the material of construction to enable visual observation of the flow phenomena. The transparent tube also facilitates the use of optical measurement technique for the identification of flow patterns. The venturimeter is installed in the test pipe at a distance of 2.5 m from the entry of the two fluids. The fluids selected are water and dyed kerosene. Their physical properties are given in Table 1. Blue dyed kerosene has been used in the experiments for better visualization of the flow phenomenon.

The venturimeter is made by machining a solid cylindrical block of transparent acrylic resin using standard design. The detailed dimensions of the venturimeter are depicted in Fig. 2. The diameter of the throat is 0.0127 m, i.e., the diameter ratio is 0.5. The converging and diverging angles are 14° and 7°, respectively.

Table 1
Physical properties of water and kerosene (at 30 °C and atmospheric pressure)

Fluid	Density (kg/m^3)	Viscosity (N s/m^2)	Surface tension (N/m)
Kerosene	792	0.0015	0.027
Water	1000	0.001	0.072

Interfacial tension ($\sigma_{O\text{-}W}$): 0.0315 N/m.

The two liquids after being pumped through previously calibrated rotameters are introduced into the test rig through a T mixer at the entry. The water and oil enter from the vertical and horizontal directions, respectively. After passing through the test section, the two-phase mixture enters a separator where they are gravity separated and directed to their respective storage tanks. The superficial velocities of both the liquids have been varied from 0.05 to 1.2 m/s. The experiments are carried out by increasing kerosene velocity at a constant water flow rate. The estimation of flow patterns and pressure drop are made simultaneously for each kerosene flow at a constant flow rate of water. The water velocity is then changed and the experiments are repeated.

2.1. Measurement technique

The measurements include identification of the flow patterns and estimation of the pressure profile over the entire range of flow velocities. Differential pressure transducers are used for pressure drop measurements. Six pairs of pressure tap (PT) are made at six locations as shown in Fig. 2. The first and second pairs are in the up-

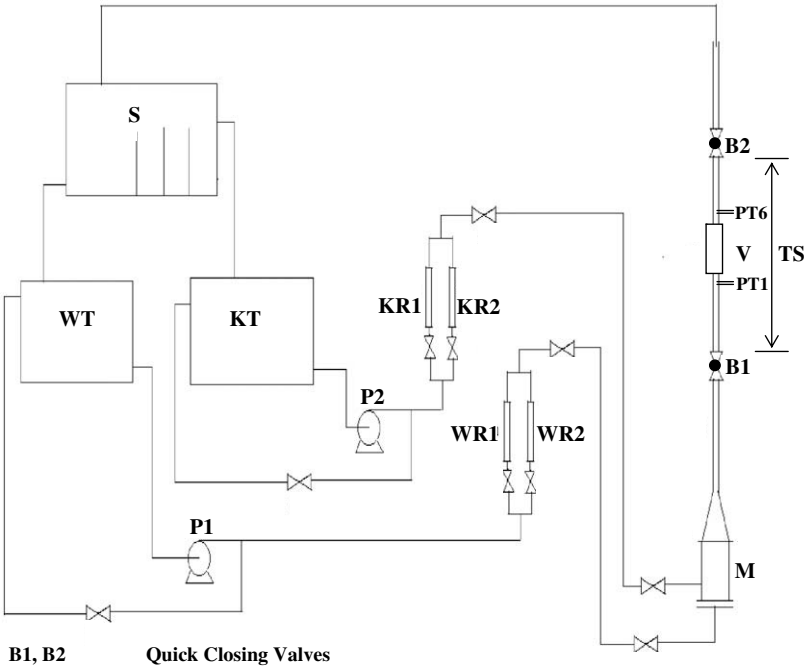

Fig. 1. Schematic diagram of the experimental setup.

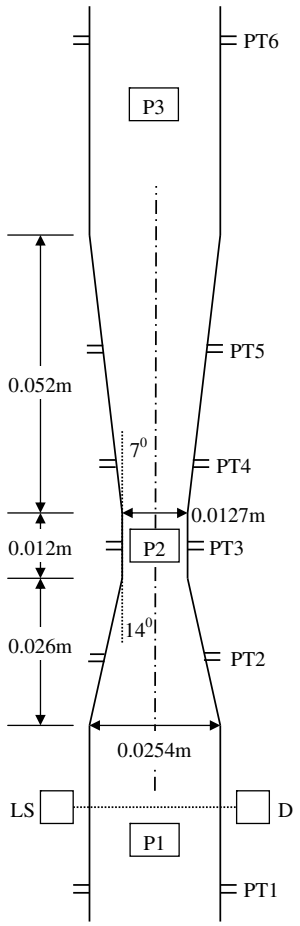

Fig. 2. Dimensions of venturimeter.

stream section at a distance of 0.074 and 0.019 m, respectively, from the middle of the venturi throat. The third pair is located at the middle of the throat and the fourth, fifth and sixth pairs are at a distance 0.015, 0.037 and 0.101 m, respectively, from the middle of the venturi throat in the downstream section. Two pressure taps are made at diametrically opposite positions at each location to ensure an average pressure at the different cross-sections.

During the present experiments care has been taken to minimize the experimental error and quantify the level of uncertainty involved. Experiments were repeated a number of times to ensure the reproducibility of the results. Calibration of the instruments were checked time to time wherever possible. Repeated measurements were also made to ascertain the properties of the test fluids.

The flow rate of the two liquids have been measured with different ranges of rotameters as mentioned earlier. The rotameters for both the liquids range from 0 to 1.67×10^{-4} m^3/s with a least count of 1.67×10^{-6} m^3/s and from 0 to 1.0×10^{-3} m^3/s with a least count of 3.33×10^{-5} m^3/s. The accuracy for the flow rate measurement using these rotameters is within ±2% as supplied by the manufacturer and also verified by in-house calibration.

To measure the pressure drop, pressure taps have been made at different distances in the flow line as mentioned earlier. Honeywell 24PCB differential pressure transducer has been used to measure the pressure drop. The transducer has a least count of 1.0×10^{-2} Pa and ±2% accuracy in the range of the experiment.

The optical probe technique as described by Jana et al. (2006a) has been used for identification of flow pattern. The signals are recorded with a frequency of 25 Hz over a period of 100 s from optical probes at three locations as shown in Fig. 2. Probes P1 and P3 are installed 0.04 m upstream and 0.06 m downstream of the venturi, respectively, and Probe P2 is installed at the venturi throat.

Due to the higher absorption coefficient of kerosene, the voltage obtained is higher for water as compared to kerosene. During the simultaneous flow of the two liquids, the voltage signals are normalized by V_{max}, the voltage value obtained when only water passes through the pipe in order to facilitate a comparative study under different flow conditions.

2.2. Analysis of the optical probe signals

The normalized probe signals are analysed using probability density function (PDF) (Jones and Zuber, 1975; Jones and Delhaye, 1976; Vince and Lahey, 1982) and wavelet analysis (Takei et al., 2000; Elperin and Klochko, 2002; Ellis et al., 2003, 2004; Briens and Ellis, 2005). The details of the analysis are mentioned in Jana et al. (2006a,b) and Chakrabarti et al. (2006). The PDF curves have been quantified by the statistical parameter namely mean (M), standard deviation (σ) and skewness (S).

The wavelet analysis is an improvement of the Fourier transform (FT) which converts a time series signal into a frequency–amplitude signal. In FT no frequency information is obtained in the time domain signal and no time information is available in the Fourier transformed signal. This deficiency in FT is resolved in wavelet transform (WT).

The wavelet transform decomposes a time series signal into different frequency level and in each frequency level a time amplitude signal is obtained. Wavelet transform is of two types – continuous wavelet transform (CWT) and discrete wavelet transform (DWT). In the present study, DWT has been used to analyse the probe signals.

In DWT the time series signal is passed through a half band digital low pass filter with impulse response $h[n]$. This process corresponds to convolution in mathematical terms. The convolution operation in discrete time is represented as

$$x[n] * h[n] = \sum_{k=-\infty}^{\infty} x[k] \cdot h[n-k] \tag{1}$$

This filtering process removes all the frequencies that are above half of the highest frequency in the signal. After this operation the signal will have half the number of data points. Hence, the scale is doubled and the procedure is mathematically represented as

$$y[n] = \sum_{k=-\infty}^{\infty} h[k] \cdot x[2n-k] \tag{2}$$

In this way the DWT analyses the signal at different frequency bands with different resolutions by decomposing the signal into detail ($d_1, d_2, \ldots, dn$) and an approximation (an). DWT employs two sets of function – scaling function and wavelet function. These two functions are associated with low pass and high pass filters, respectively. The decomposition of the signal into different frequency bands is done by successive high pass and low pass filtering of the signal. The original signal $x[n]$ is first passed through a half band high pass filter $g[n]$ and a low pass filter $h[n]$. This constitutes the first level of decomposition and mathematically this can be represented as

$$y_{high}[k] = \sum_{n} x[n] \cdot g[2k-n] \tag{3}$$

$$y_{low}[k] = \sum_{n} x[n] \cdot h[2k-n] \tag{4}$$

where $y_{high}[k]$ and $y_{low}[k]$ denote the outputs of the high pass and low pass filters, respectively, after sub-sampling by 2. In the second and subsequent level the approximation or the low-frequency components of the previous level is treated in the similar way as done in the first level.

For the wavelet analysis, the Daubechies 4 with level 5 has been adopted to decompose the normalized probe signals into five different frequency levels. In the analysis d_1 denotes the smallest scale and highest frequency band; d_2, d_3, etc. represent progressively lower frequency band and the approximation a_5 reflects the large scale resolution. In the present study standard deviations have been calculated for the five details (d_1–d_5) and the lowest frequency approximation (a_5) to characterize the distribution of the phases in the three sections.

The above discussions reveal that study of the hydrodynamics of liquid–liquid flow through venturi has been carried out using different measurement techniques. Some of these measurements are direct (like flow rate and pressure drop) while the others are indirect like the signal of the optical probe and different statistical parameters extracted from them. These are indirect in the sense that they characterize the type of flow phenomena which occur over a range. Though the absolute values of these 'indirect' parameters are not important, the pattern of their variation and the associated ranges are meaningful for any characterization process. In general these parameters are obtained from digital signal processing and possess a high level of accuracy. Nevertheless, it would be prudent to examine whether the accuracy/uncertainty of these parameters can bias the characterization of flow. To calculate PDF a least count (bin size) has been selected in the range 0.05–0.0005 depending on the standard deviation of the signal. Thus the error associated with it is negligibly small.

3. Results and discussion

It may be noted that flow distribution in the present pipeline could not be observed visually except at low phase velocities. The passage appeared to be blue or bluish white for most of the conditions. So we had to rely on the signals obtained from the optical probes and the quantitative measures of the PDFs for a useful guide to estimate the different regimes. The probe signals have been validated with visual observations of the phase distribution for kerosene–water flow through horizontal pipes. The information thus obtained is reported in Chakrabarti et al. (2006, 2007) and used in the present study to understand the flow regimes from the probe signals upstream and downstream of the venturi. Moreover, a comparison of the PDFs with the observations made by Jana et al. (2006a,b) have further enabled us to identify the transitions between the different patterns at a particular section and the differences in flow distribution between the upstream and downstream regions of the venturimeter.

3.1. Flow patterns from the probe signals and PDF analysis

The probe signals and the corresponding PDF curves for three different water velocities have been presented in a tabular form in Figs. 3 and 4. Each figure depicts the situation at a constant water and increasing kerosene velocity. The rows of the figure are numbered as 3.1, 3.2, etc. They represent the situation at a constant flow rate of the two liquids. The depiction is made in five parts. The first three columns (a)–(c) show the probe signals at the upstream, throat and downstream sections, respectively. The corresponding PDFs for all the signals are presented in a single figure in column (d) to facilitate a comparative study and note the influence of the venturi on the interfacial distribution. The PDFs have been quantified by mean, standard deviation and skewness and these are denoted by M, σ and S, respectively, in column (e). In Figs. 3–6 the flow pattern labels have been shown as B, DB, CT, CA and ID to denote bubbly, dispersed bubbly, churn turbulent, core annular and inverted dispersed pattern, respectively.

Fig. 3 shows that the flow is bubbly at low phase velocities (U_{SW} = 0.05 m/s, U_{SK} = 0.05 m/s). In this flow pattern kerosene is dispersed as discrete droplets in the continuous water medium and resembles the bubbly flow pattern of gas–liquid flows. It may be noted that Jana et al. (2006a) reported similar PDF characteristics in the bubbly flow pattern through a vertical tube. This is marked by a unimodal PDF at high voltage values (V/V_{max} > 0.85),

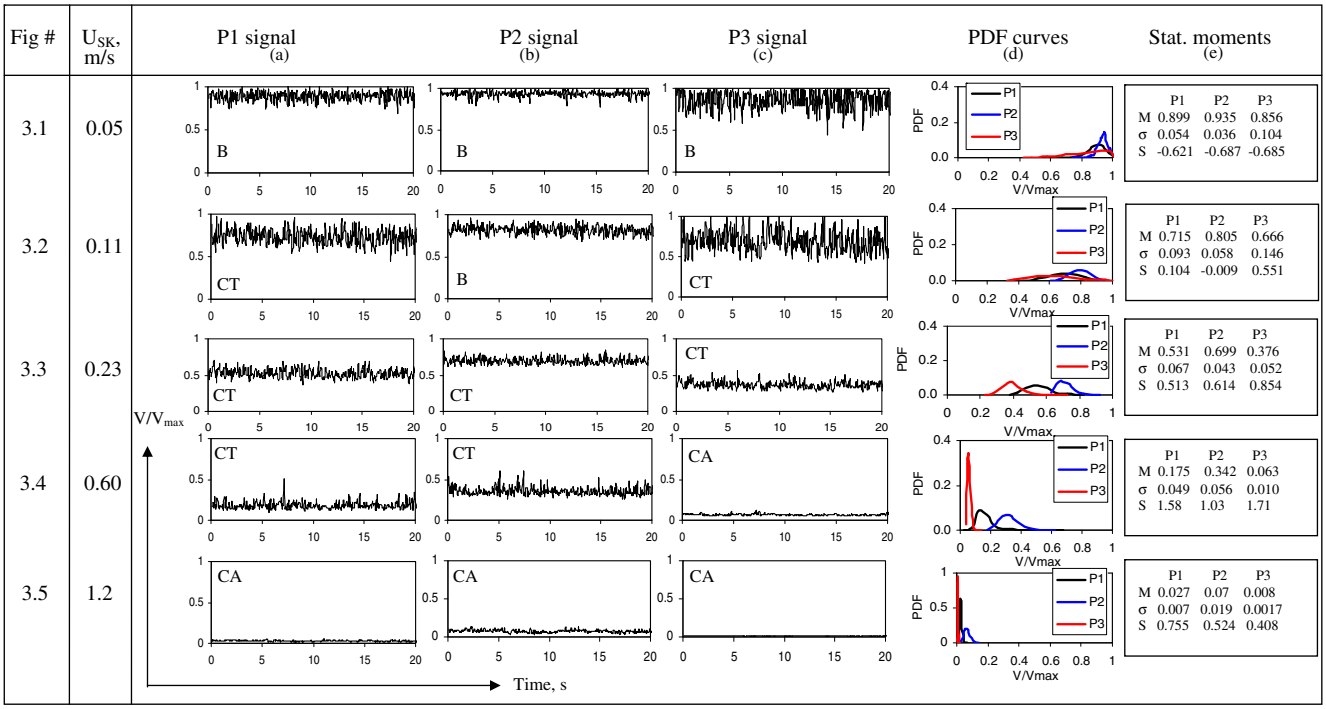

Fig. 3. Probe signals and their PDFs at U_{SW} = 0.05 m/s.

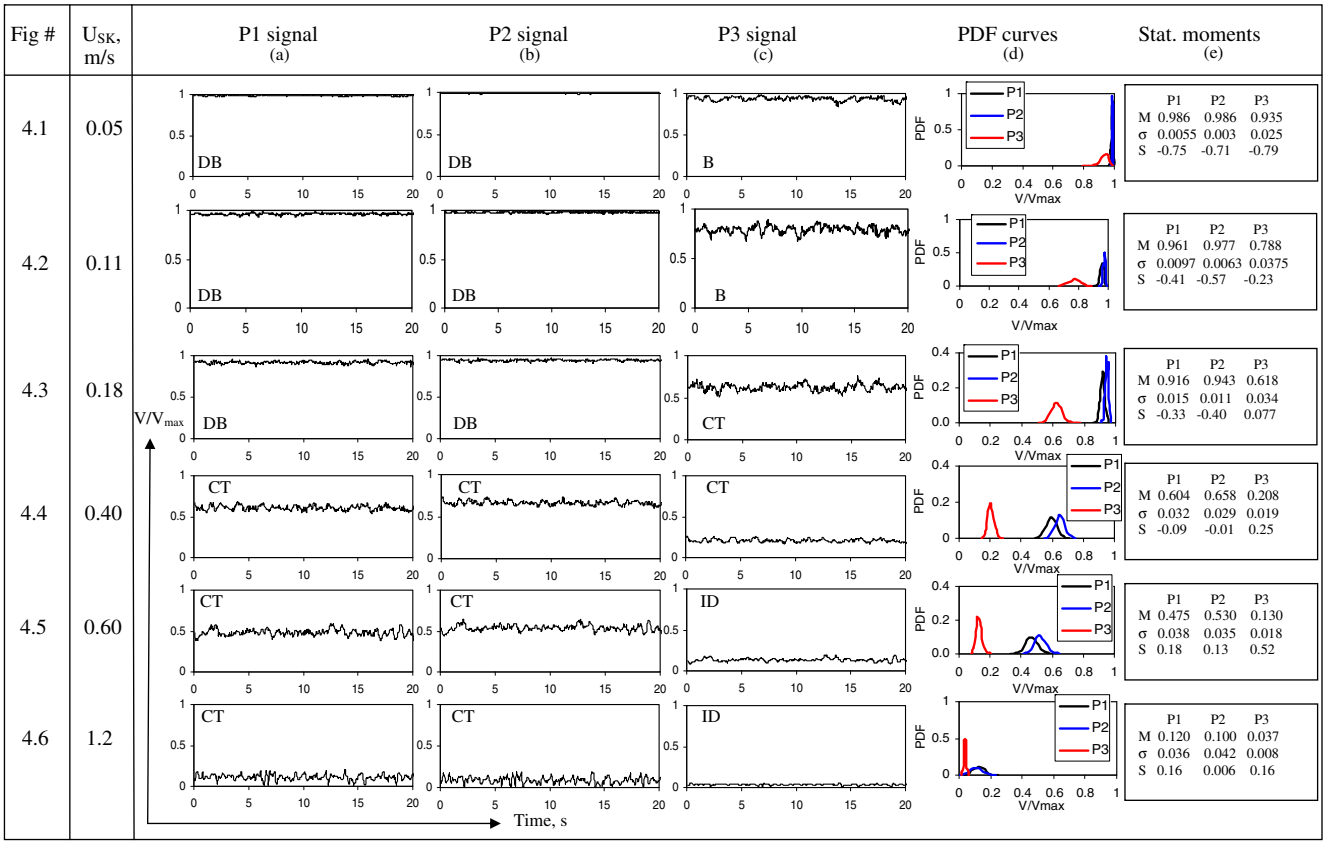

Fig. 4. Probe signals and their PDFs at U_{SW} = 1.2 m/s.

significant spread and negative skewness at all the three sections of the pipeline. Fig. 3.1 shows that the fluctuations of the probe signals decrease at the throat and increase at the downstream section. This can probably be attributed to the accelerated flow of the bubbly mixture thus resulting in reduced scattering of light in the converging section, while the reverse phenomenon occurs in the diverging section.

With increase in kerosene velocity (from 0.05 to 0.11 m/s) at a constant water flow rate (U_{SW} = 0.05 m/s), the mean value of the three probe signals decrease as expected while the fluctuations in all the three cases increase. This is manifested by an increased spread in all the PDF curves of Fig. 3.2 and arises due to an increase in the size and frequency of kerosene drops. However, the visual observations under these conditions do not give a clear picture of the interfacial distributions. It merely reveals the oil phase to exist as irregular chunks in the continuous water medium and a continuously changing interface between them. Moreover, the skewness changes from negative to positive for probes P1 and P3 but remains negative for probe P2. Jana et al. (2006a) had attributed the shift of skewness to a change of the dominating phase from water to oil. In this case, it indicates the onset of churn-turbulent flow at the two positions while the situation at the throat appears to retain bubbly characteristics. It exhibits churn-turbulent flow at higher kerosene velocities.

Henceforth, a further increase in kerosene velocity is accompanied by a shift of the unimodal PDF towards lower V/V_{max} and a reduction in its spread. The skewness remains positive for all the cases. As the kerosene flow rate is increased further, the pattern is indicated by an almost straight line PDF at $V/V_{max} < 0.2$ and negligible spread. This suggests core annular flow with kerosene flowing through center of the pipe and water as a thin film between kerosene core and pipe wall. The transition occurs at lower kerosene velocities in the downstream section and is followed by the transition at the upstream and subsequently at the throat of the venturi.

The experiments have been performed for several constant velocities of water and the results show similar trend at higher water velocities. The flow is initially bubbly in all sections of the pipeline and is manifested by a high V/V_{max} (>0.85) and negative skewness. The spread is significant ($\sigma > 0.05$) for the probe signals at upstream and downstream section while it is much less ($\sigma \geqslant 0.03$) at the throat. For bubbly flow, the spread is consistently higher for probe P3 and the lowest for probe P2. This brings out the influence of the converging and diverging sections on liquid–liquid bubbly flow through vertical pipes. An increase in kerosene velocity exerts a twofold influence on the PDF curves. It shifts the PDFs to lower voltages and increases their spread. The reason behind this can be attributed to the combined effect of decreased attenuation as well as increased scattering thus denoting an increase in the frequency and size of the discontinuous phase with increase in oil flow rate. This continues till the flow becomes a chaotic random mixture of the two liquids and enters churn-turbulent flow. Since it is difficult to visualize the transition, a change in the sign of skewness with V/V_{max} being less than 0.7 has been selected as the criteria to identify the transition. It is expected that the aforementioned criteria represent a tendency of the continuous phase to shift from water to kerosene as has also been mentioned by Jana et al. (2006a). With a further increase in kerosene velocity, both the voltage and the spread gradually decrease and the onset of core annular flow is represented by an almost straight line PDF at $V/V_{max} < 0.2$ and $\sigma < 0.01$. Nevertheless, all the transitions have been noted to occur first in the downstream section followed by the upstream and the throat region. Moreover, under these conditions, the flow as indicated by probes P1 and P2 do not attained

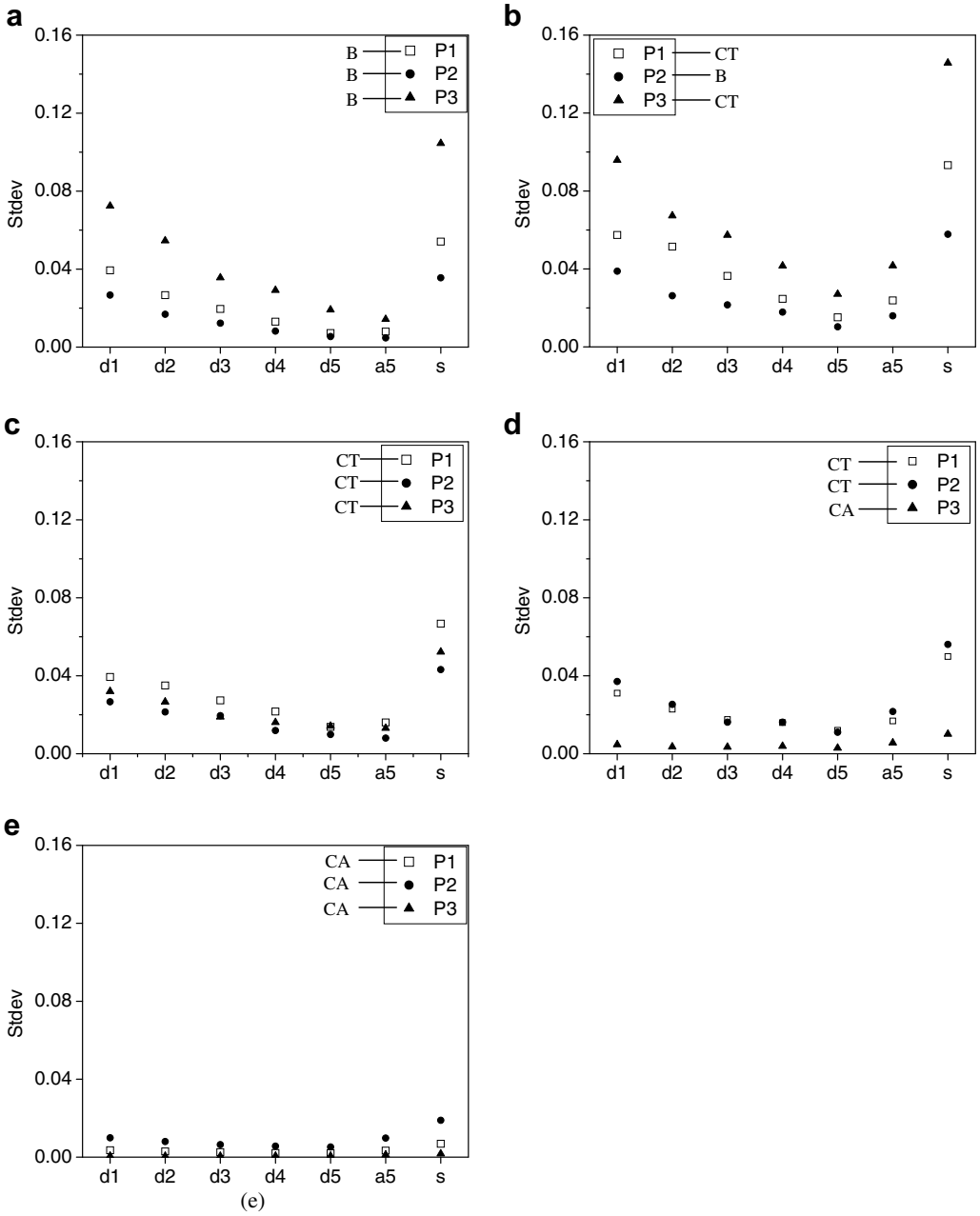

Fig. 5. Standard deviations at U_{SW} = 0.05 m/s for (a) U_{SK} = 0.05 m/s; (b) U_{SK} = 0.11 m/s; (c) U_{SK} = 0.23 m/s; (d) U_{SK} = 0.6 m/s and (e) U_{SK} = 1.2 m/s.

core annular characteristics over the entire range of phase flow rates while the reduced phase velocities in the diverging section has enabled coalescence of kerosene chunks and a continuous kerosene core at probe P3 for higher oil flow rates.

The situation changes drastically at still higher water velocities ($U_{SW} \geqslant 0.9$ m/s). At low oil flows, kerosene is observed to be finely dispersed in the continuous water medium as shown in Fig. 4.1. This is denoted by a PDF at $V/V_{max} > 0.9$ and a negligible spread in agreement to the observations of Jana et al. (2006a). The spread is higher for probe P3 and increases slightly with increase in kerosene flow rate till the skewness shifts its sign. Subsequently, the signal fluctuations and the PDF spread decreases in agreement to the observations at lower water flow rates. On the contrary, the fluctuations in the signals of probes P1 and P2 and the spread in the corresponding PDFs increase with kerosene velocity throughout the entire range of phase flow rates even after the skewness changes its sign. The flow passage assumes a bluish white appearance under such conditions at high kerosene flows. It may be noted that a more detailed description of flow patterns is available in Jana et al. (2006a,b) and Chakrabarti et al. (2006, 2007).

3.2. Wavelet analysis

It is evident from the aforementioned discussion that the PDFs can provide an idea regarding the gross distribution of the two liquids under different flow conditions. However, they do not throw much light on the intrinsic changes in the flow details which bring out the transition between the different flow patterns. Moreover, they fail to discern the flow distributions at higher phase velocities. With these considerations, the wavelet analysis has been adopted for a better appraisal of the flow phenomenon.

This analysis not only confirms the inferences drawn from the PDF curves at low to moderate velocities but also enables us to

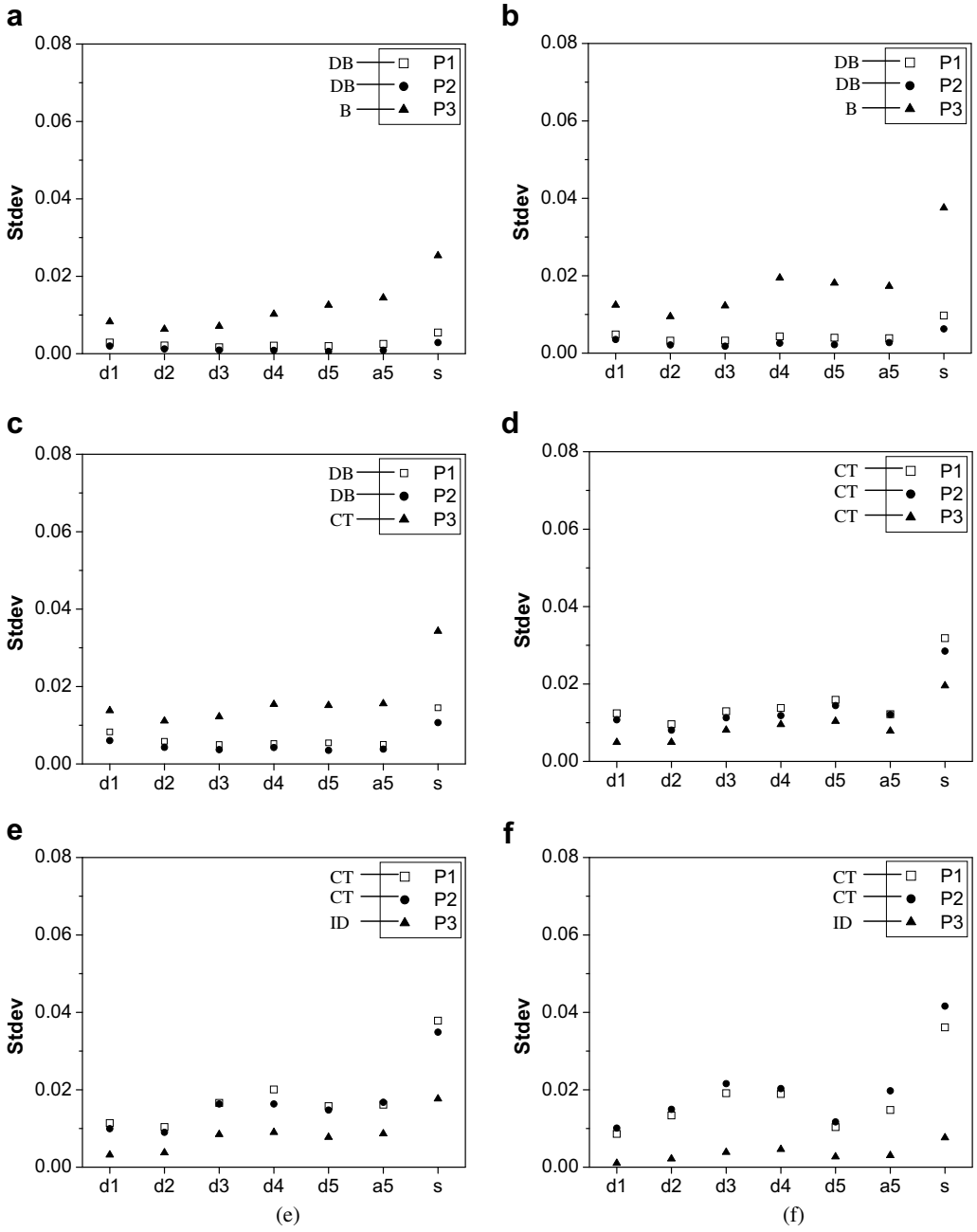

Fig. 6. Standard deviations at U_{SW} = 1.2 m/s for (a) U_{SK} = 0.05 m/s; (b) U_{SK} = 0.11 m/s; (c) U_{SK} = 0.18 m/s; (d) U_{SK} = 0.4 m/s; (e) U_{SK} = 0.6 m/s and (f) U_{SK} = 1.2 m/s.

understand the interfacial configurations at high phase flow rates, where the PDFs could not offer a suitable description.

As mentioned earlier, the Daubechies 4 wavelet with level 5 has been adopted for this purpose. For a compact and complete representation, the results have been presented as the standard deviation at the different levels of detail (d_1–d_5) and approximation (a_5) for different constant velocities of the two liquids. It is expected that the fluctuations at the high-frequency levels occur due to scattering of light by the bubbles/discontinuous phase while a large spread at the lower frequency bands and large scale resolution (a_5) occurs due to interfacial waviness. The analysis of the signals given in the column (a) of Figs. 3 and 4 has been presented in Figs. 5 and 6.

Fig. 5(a) shows that bubbly flow is denoted by higher fluctuations at d_1 and progressively lower spread at the higher levels. The onset of churn-turbulent flow is denoted by an increase in fluctuations at all levels thus hinting at the increase in randomness of the mixture. Interestingly a_5 appears to be slightly higher than d_5 for the majority of the churn-turbulent flow situations and this indicates an increase in the size of the discontinuous phase as well as the appearance of interfacial waviness. It is evident from Fig. 5(a) and (b) that the increased PDF spread of probe P3 in Figs. 3.1 and 3.2 is due to higher fluctuations at d_1 level as compared to the other levels. This confirms that an increase in the size and frequency of the bubbles has caused the higher fluctuations in the signal of probe P3. Similarly, the decrease in the spread for all the probe signals with increase in kerosene velocity in the churn-turbulent flow pattern and a smaller spread of probe P3 as compared to the other probes under these conditions also occur primarily due to a reduction in the d_1 fluctuations as compared

to the fluctuations in the lower frequencies and the approximation (a_5) of the decomposed signal. It may be noted that core annular flow is denoted by negligible fluctuations at all levels thus indicating a separated flow with a more or less smooth interface. Moreover, the standard deviation of d_1–d_5 and a_5 are of the same order of magnitude in this pattern unlike bubbly and churn-turbulent flow, which are characterized by higher standard deviations at d_1. This difference is particularly evident from Fig. 5(d) where probes P1 and P2 exhibit churn-turbulent flow while probe P3 denotes core annular characteristics.

Fig. 6 shows that the wavelet analysis yields different results for the bubbly and dispersed bubbly flow patterns. Bubbly flow pattern was characterized by high fluctuations at d_1 and gradually decreasing standard deviation at the lower frequency levels and approximation. The reverse situation is observed during dispersed flow [Fig. 6(a)]. Although there is very less difference between the fluctuations at the different levels, the standard deviation appears to be higher for low-frequency levels and approximation as compared to that at the highest frequency band. This can be attributed to the rapid propagation of the dense array of fine droplets, which form a homogeneous mixture in the continuous water medium. Fig. 6(a) clearly indicates that the small PDF spread for probes P1 and P2 in Fig. 4.1(d) arises due to the negligible fluctuations at all the levels of frequency and an increase in the standard deviation at all levels contributes to the increased standard deviation for probe P3. Subsequently, with increase in kerosene velocity the spread at the different levels assume a different trend for probe P3 in the region where the skewness gradually changes from a negative to positive sign. Henceforth, the fluctuations continue to decrease with increase in kerosene velocity although it exhibits higher spread at lower frequency levels. An identical situation is observed for probes P1 and P2 but at much higher kerosene velocities [Fig. 6(e) and (f)].

From the aforementioned discussion, it is evident that the inception of churn-turbulent flow as indicated by higher fluctuations at lower frequency bands occurs due to the coalescence of kerosene. On further increase of kerosene velocity, the fluctuations not only decrease at all levels but the trend of variation of σ with the level of decomposition also appears to be different. It may be noted that core annular flow cannot occur at such high water velocities and the flow passage has oil as the predominating phase ($M < 0.2$). A comparison of the wavelets with those reported by Chakrabarti et al. (2006) during phase inversion indicates that similar results marked the transition from kerosene dispersed to water dispersed pattern under similar flow conditions. It can therefore, be deduced that the flow at high kerosene velocities marked by $V/V_{max} < 0.2$, positive skewness and a higher standard deviation for lower frequency bands marks inverted dispersed flow.

Thus Figs. 4 and 6 show that the flow is dispersed bubbly throughout the pipeline at low kerosene flows with a larger size and frequency of the drops in the downstream section. As the kerosene flow is increased, the droplets coalesce to form the erratic churn-turbulent flow pattern, which is marked by positive skewness and V/V_{max} less than 0.6. However, the standard deviation at the different levels does not follow the same trend as observed for churn-turbulent flow at lower water velocities (Fig. 5) probably due to the small size of droplets and a more mixed character of flow. With a further increase in kerosene velocity, the discontinuous phase tends to invert to form the continuous medium and vice versa. The nature of the curves in Fig. 4(d) and (e) indicate that while phase inversion has occurred at probe P3, the situation at the upstream and the throat region lies in the churn-turbulent regime with kerosene coalescing to form the continuous phase in the entire range of flow velocities studied. It may be noted that the previous researchers (Arashmid and Jeffreys, 1980; Brauner and Ullmann, 2002; Liu et al., 2005; Chakrabarti et al., 2006) have named the transition region between dispersed and inverted dispersed flow as the ambivalent region. In the present study this regime is named as churn-turbulent flow to maintain a minimum of flow patterns but the PDFs and wavelets do show certain differences in the characteristics of churn-turbulent flow at lower and higher water velocities.

3.3. Flow pattern map at the upstream and the downstream section of the venturi

Attempts have next been made to classify the interfacial configurations as observed at the upstream and downstream sections into different flow patterns. Since visual observations have failed to provide any useful information, the patterns have been classified on the basis of the PDF characteristics (M, σ and S) and wavelet analysis. At low phase velocities, bubbly flow is characterized by a high peak at high V/V_{max} ($M > 0.7$), significant spread ($\sigma > 0.05$) and negative skewness. The droplets are cap shaped or oblate spheroidal and resemble the bubbly flow pattern in gas–liquid flows. The dispersed flow pattern where kerosene is finely dispersed in water medium is observed at high water and low kerosene velocity and is indicated by a mean at $V/V_{max} > 0.9$, low spread ($\sigma < 0.015$) and negative skewness. During the passage of the liquid mixture through the diverging section of the venturi, coalescence of the tiny kerosene droplets take place. As a result larger drops of kerosene are noted in the downstream section. This results in increased scattering and is indicated by a shift of the PDF to lower voltage values and a higher spread. The core annular flow pattern at high kerosene and low water velocity is characterized by a unimodal PDF at low V/V_{max} ($M < 0.2$), low spread ($\sigma < 0.01$) and positive skewness. The transition from bubbly to core annular flow occurs via the churn-turbulent flow pattern. This is characterized by $M < 0.6$, very high standard deviation ($0.05 < \sigma < 0.15$) and a shift of skewness from negative to positive value. The PDF spread is noted to be the highest in the churn-turbulent flow pattern.

The situation becomes different at high water velocities ($U_{SW} \geqslant 0.9$ m/s). The flow does not exhibit core annular characteristics with increase in kerosene velocity. On the contrary, the water gets dispersed in the continuous kerosene. This has been named as inverted dispersed flow and is characterized by a unimodal PDF at $V/V_{max} < 0.2$, a small spread ($\sigma < 0.015$) similar to that observed for dispersed flows and a positive skewness. It may be noted that the PDF characteristics of inverted flow often appear to be similar to those observed for core annular flow. However, the wavelet analysis brings out the difference between the flow distributions. In core annular flow the standard deviations of five details (d_1–d_5) and a_5 are much less and similar in magnitude while for the inverted dispersed pattern the standard deviation is higher for lower frequency bands. The quantitative measures of the PDFs and the variation of standard deviation at the different levels and approximation of the wavelet resolution are listed in Table 2 for different flow patterns. Based on this flow pattern maps have been constructed for the upstream and downstream sections and presented in Fig. 7(a) and (b). A comparison between the two figures brings out the differences in the range of existence of the different regimes at the two sides of the venturimeter. The dispersed bubbly flow pattern is not observed in the downstream region over the range of flow conditions studied.

3.4. Pressure drop profile

The pressure drop has been measured at five positions with respect to the first pressure tap (0.074 m upstream from the throat) and represented in Fig. 8 at three constant velocities of water. In the three graphs of Fig. 8 the zero position along the pipe axis indicates the mid point of the venturi throat. All the three

Table 2
PDF moments and wavelet analysis in different flow patterns

Flow pattern	M	σ	S	Nature of five details and a_5
(i) Bubbly	>0.7	>0.05	Negative	σ decreases from d_1 to d_5 and a_5
(ii) Churn	<0.7	$0.05 < \sigma < 0.15$	Positive	σ is higher for d_1 to d_5 and a_5
(iii) Core annular	<0.2	<0.01	Positive	σ is very low and almost same for all d_1 to d_5 and a_5
(iv) Dispersed	>0.9	<0.015	Negative	σ is very low and almost same for all d_1 to d_5 and a_5
(v) Inverted dispersed	<0.2	<0.015	Positive	σ is higher for d_4

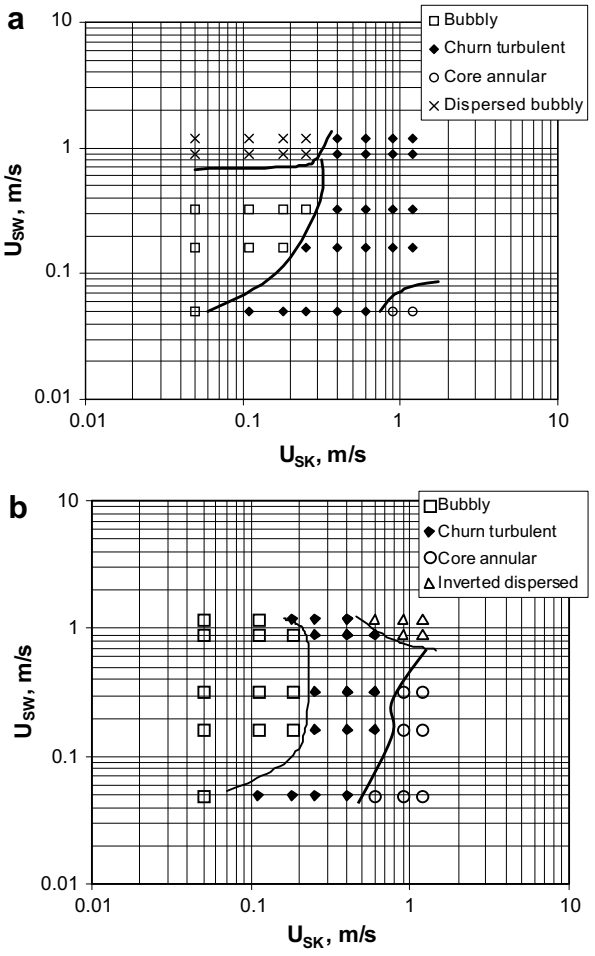

Fig. 7. Flow pattern map in (a) upstream and (b) downstream section.

plots depict a similar nature of the curve of pressure drop versus position along pipe axis. They show that the pressure drop is maximum at the throat and it decreases in the downstream section. This is due to the fact that during the flow of the two-phase mixture through the venturimeter, the mixture attains the maximum average velocity at the throat. Subsequently, the velocity decreases gradually in the diverging section. During this change in velocity, the velocity head is converted to pressure head which is reflected in Fig. 8. Further as the water velocity is increased, the pressure drop increases an agreement to the pressure drop profile observed for single-phase flows.

3.5. Measurement of two-phase mass flow rate

Attempts have next been made to estimate the two-phase mass flow rate from pressure drop measurement using the following equation based on the mixture density viz.

$$Q = \frac{A_2 C_D}{\sqrt{1-(A_2/A_1)^2}}\left(\frac{2\Delta p}{\rho_m}\right)^{1/2} \tag{5}$$

In the above equation Q is the volumetric flow rate as measured by a rotameter, A_2 and A_1 are the area of throat and pipe, respectively, Δp the pressure difference between upstream and throat, ρ_m the mixture density and C_D is the discharge coefficient. It has been noted to vary between 0.98 and 0.99 for flow of water only through the venturimeter of the present experiments. To calculate C_D in different flow patterns from known total flow rate (measured by rotameter), the mixture density ρ_m has been taken as the homogeneous density of the liquid mixture, which is expressed in terms of densities of the individual fluids as

$$\rho_m = (1-\beta)\rho_O + \beta\rho_W \tag{6}$$

where ρ_O and ρ_W are the densities of oil and water, respectively, and β is the inlet volume fraction of water given by

$$\beta = \frac{U_{SW}}{U_{SW}+U_{SK}} \tag{7}$$

To estimate the uncertainty on C_D from Eq. (5), the same equation can be written as

$$C_D = f(Q, \Delta p, \rho_m) \tag{8}$$

Therefore, uncertainty in C_D is expressed as (Holman, 1989)

$$\delta C_D = \left[\left(\frac{\partial C_D}{\partial Q}\delta Q\right)^2 + \left(\frac{\partial C_D}{\partial(\Delta p)}\delta(\Delta p)\right)^2 + \left(\frac{\partial C_D}{\partial \rho_m}\delta\rho_m\right)^2\right]^{1/2} \tag{9}$$

where the errors in the estimation of flow rate, pressure and mixture density are given by δQ, $\delta(\Delta p)$ and $\delta\rho_m$, respectively. Based on the above equation one gets a maximum uncertainty of 2.87% in C_D for two-phase condition.

However, it should be noted that the mixture density has been estimated based on homogeneous flow model and in the absence of knowledge of in situ volume fraction, the inlet volume fraction has been used in the calculation.

The variation of C_D values as calculated in the different flow patterns has been presented in Fig. 9. The figure shows that the values are closest to the value obtained for water only in the dispersed flow pattern and it is the lowest in core annular flow. It is interesting to note that homogeneous equilibrium model is most suitable for dispersed flow while it is least appropriate for core annular flow. Moreover, there is some variation of C_D in the bubbly and churn-turbulent flow patterns.

In order to reduce this range of variation, attempts have been made to use the drift-flux model to predict ρ_M in the aforementioned flow distributions. The model modifies the in situ water holdup (H_W) obtained from the homogeneous theory by incorporating the relative motion between the two phases. This yields the expression of H_W as

$$H_W = \frac{j_1 + j_{21}}{j} \tag{10}$$

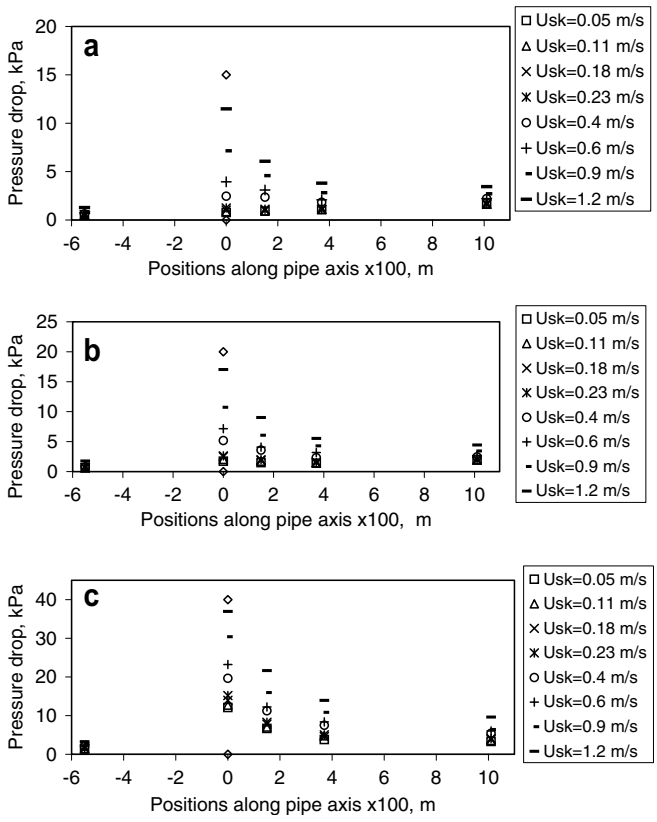

Fig. 8. Plot of pressure drops at (a) $U_{SW} = 0.05$ m/s; (b) $U_{SW} = 0.3$ m/s and (c) $U_{SW} = 1.2$ m/s.

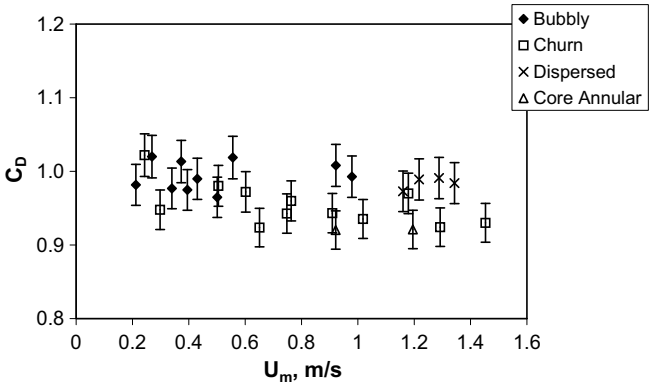

Fig. 9. Plot of C_D in different flow patterns using homogeneous density.

where j_1, j_{21} and j are volumetric flux of phase 1 (water), drift flux and volumetric flux of two-phase mixture, respectively. For gravity dominated flow j_{21} is obtained from Wallis (1969) as

$$j_{21} = U_\infty \alpha (1-\alpha)^n \tag{11}$$

The expressions for U_∞ and n for the bubbly flow and churn-turbulent flow patterns have been adopted from the table provided by Peebles and Garber (1953) as given in Wallis (1969) viz.

$$U_\infty = 1.18\left(\frac{g\sigma}{\rho_W}\right)^{0.25} \quad \text{and} \quad n = 2 \text{ for bubbly flow pattern} \tag{12}$$

and

$$U_\infty = 1.53\left[\frac{g\sigma\Delta\rho}{\rho_W^2}\right]^{0.25} \quad \text{and} \quad n = 0 \text{ for churn-turbulent flow pattern} \tag{13}$$

On substituting Eqs. (12) and (13) in Eq. (11), we obtain the value of drift flux (j_{21}) and this gives us the value of water holdup (H_W) from Eq. (10). The value of H_W when substituted in the expression of ρ_M viz.

$$\rho_M = H_W\rho_W + (1-H_W)\rho_O \tag{14}$$

gives C_D from Eq. (5).

The C_D values thus calculated in the bubbly and churn-turbulent flows using mixture density from drift-flux model shows a marginal improvement due to the improved value of mixture density. The value of C_D in the former case was observed to lie between 0.924 and 1.022 whereas the range reduced to 1.009–0.927 when the mixture density was calculated using drift-flux model.

4. Conclusion

The flow patterns in the upstream of venturi in the present work differ significantly from those observed by Jana et al. (2006a). In both the cases sufficient lengths have been provided for attaining fully developed flow. The only factor which appears to influence the flow pattern in the upstream is the proximity to the converging section. It may be noted that the measuring point in the upstream is at a distance of 0.04 m ($L/D = 1.54$) only from the venturi. This fact must be accounted for development of models to predict the hydrodynamics of flow. For example, a model developed for churn flow at the upstream will not be able to predict the parameters in the downstream region where the flow exhibits core annular characteristics. The venturimeter has also been used to measure the two-phase mass flow meter.

The following observations have been made in the present work:

- The presence of venturimeter is observed to influence the phase distribution primarily in the upstream section. However, the pattern transitions are observed to occur at lower velocities in the downstream section.
- Finely dispersed bubbles are not observed in the downstream section due to coalescence of tiny kerosene droplets during its passage through the converging and diverging section.
- Inverted dispersed flow appears only in the downstream and not in the upstream section in the range of flow rates studied.
- The venturimeter can be used to measure the mass flow rate for different oil–water pairs using the homogeneous/drift-flux model since the majority of oils have densities close to that of water. However, fresh calibration is necessary while using high viscosity oils.
- A separate analysis is required for core-annular pattern at the upstream section. This has not been tried in the present work due to insufficient data in this regime.
- The value of C_D does not differ significantly for the different flow regimes in the present case and it is close to the value for single phase water flow through the venturimeter.

Acknowledgement

The authors are grateful to Department of Science and Technology, India for providing financial support for the work.

References

Angeli, P., Hewitt, G.F., 1998. Pressure gradient in liquid–liquid flows. Int. J. Multiphase Flow 24, 183–1203.
Angeli, P., Hewitt, G.F., 2000. Flow structure in horizontal oil–water flow. Int. J. Multiphase Flow 26, 1117–1140.

Arashmid, M., Jeffreys, G.V., 1980. Analysis of the phase inversion characteristics of liquid–liquid dispersions. AIChE J. 26, 51–55.
Boyer, C., Lemonnier, H., 1996. Design of a flow metering process for two-phase dispersed flows. Int. J. Multiphase Flow 22, 713–732.
Brauner, N., 2001. The prediction of dispersed flows boundaries in liquid–liquid and gas–liquid systems. Int. J. Multiphase Flow 27, 885–910.
Brauner, N., Ullmann, A., 2002. Modelling of phase inversion phenomenon in two-phase pipe flow. Int. J. Multiphase Flow 28, 1177–1204.
Briens, L.A., Ellis, N., 2005. Hydrodynamics of three-phase fluidized bed systems examined by statistical, fractal, chaos and wavelet analysis methods. Chem. Eng. Sci. 60, 6094–6104.
Brown, R.A.S., Govier, G.W., 1961. High-speed photography in the study of two-phase flow. Can. J. Chem. Eng. 39, 159–164.
Chakrabarti, D.P., Das, G., Das, P.K., 2006. The transition from water continuous to oil continuous flow pattern. AIChE J. 52, 3668–3678.
Chakrabarti, D.P., Das, G., Das, P.K., 2007. Identification of stratified liquid–liquid flow through horizontal pipes by a non-intrusive optical probe. Chem. Eng. Sci. 62, 1861–1876.
Charles, M.E., Govier, G.W., Hodgson, G.W., 1961. The horizontal pipeline flow of equal density oil–water mixture. Can. J. Chem. Eng. 39, 27–36.
Ellis, N., Briens, L.A., Grace, J.R., Bi, H.T., Lim, C.J., 2003. Characterization of dynamic behaviour in gas–solid turbulent fluidized bed using chaos and wavelet analyses. Chem. Eng. J. 96, 105–116.
Ellis, N., Bi, H.T., Lim, C.J., Grace, J.R., 2004. Influence of probe scale and analysis method on measured hydrodynamic properties of gas-fluidized beds. Chem. Eng. Sci. 59, 1841–1851.
Elperin, T., Klochko, M., 2002. Flow regime identification in a two-phase flow using wavelet transform. Exp. Fluids 32, 674–682.
Farrar, B., Bruun, H.H., 1996. A computer based hot-film technique used for flow measurements in a vertical kerosene–water pipe flow. Int. J. Multiphase Flow 22, 733–751.
Gaston, M.J., Reizes, J.A., 2001. Evans GM. Modeling of bubble dynamics in a venturi flow with a potential flow method. Chem. Eng. Sci. 56, 6427–6435.
Govier, G.W., Sullivan, G.A., Wood, R.K., 1961. The upward vertical flow of oil–water mixtures. Can. J. Chem. Eng. 9, 67–75.
Guzhov, A., Grishin, A.D., Medredev, V.F., Medredeva, O.P., 1973. Emulsion formation during the flow of two liquids in a pipe. Neft. Khoz. 8, 58–61 (in Russian).
Holman, J.P., 1989. Experimental Methods for Engineers, fifth ed. McGraw-Hill, New York.
Hu, B., Angeli, P., 2006. Phase inversion and associated phenomena in oil–water vertical pipeline flow. Can. J. Chem. Eng. 84, 94–107.
Huang, X., Sciver, S.W.V., 1996. Performance of a venturi flow meter in two-phase helium flow. Cryogenics 36, 303–309.
Huang, Z., Xie, D., Zhang, H., Li, H., 2005. Gas–oil two-phase flow measurement using an electrical capacitance tomography system and a venturi meter. Flow Meas. Instrum. 16, 177–182.
Ioannou, K., Hu, B., Matar, Omar K., Hewitt, G.F., Angeli, P., 2004. Phase inversion in dispersed liquid–liquid pipe flows. In: Proceedings of the 5th International Conference on Multiphase Flow, ICMF'04, Yokohama, Japan, May 30–June 4, Paper No. 108.
Ioannou, K., Nydal, Ole J., Angeli, P., 2005. Phase inversion in dispersed liquid–liquid flows. Exp. Therm. Fluid Sci. 29, 331–339.
Jana, A.K., Das, G., Das, P.K., 2006a. A novel technique to identify flow patterns during liquid–liquid two-phase upflow through a vertical pipe. Ind. Eng. Chem. Res. 45, 2381–2393.
Jana, A.K., Das, G., Das, P.K., 2006b. Flow regime identification of two-phase liquid–liquid upflow through vertical pipe. Chem. Eng. Sci. 61, 1500–1515.
Jana, A.K., Mandal, T.K., Chakrabarti, D.P., Das, G., Das, P.K., 2007. An optical probe for liquid–liquid two-phase flows. Meas. Sci. Technol. 18, 1562–1575.
Jones, O.C., Delhaye, J.M., 1976. Transient and statistical measurement techniques for two-phase flows: a critical review. Int. J. Multiphase Flow 3, 89–116.
Jones, O.C., Zuber, N., 1975. The interrelation between void fraction fluctuations and flow pattern in two-phase flow. Int. J. Multiphase Flow 2, 273–306.
Katheder, H., Susser, M., 1989. Discharge coefficient of a classical venturi tube for measuring liquid helium flow. Cryogenics 29, 1067–1069.
Liu, L., Matar, O.K., Ortiz, E.S.P.D., Hewitt, G.F., 2005. Experimental investigation of phase inversion in a stirred vessel using LIF. Chemical Engineering Science, vol. 60, pp. 85–94.
Lovick, J., Angeli, P., 2004. Experimental studies on the dual continuous flow pattern in oil–water flows. Int. J. Multiphase Flow 30, 139–157.
Oddie, G., Pearson, J.R.A., 2004. Flow-rate measurement in two-phase flow. Annu. Rev. Fluid Mech. 36, 149–172.
Pal, R., 1993. Flow of oil-in-water emulsions through orifice and venturi meters. Ind. Eng. Chem. Res. 32, 1212–1217.
Peebles, F.N., Garber, H.J., 1953. Studies on the motion of the gas bubbles in liquid. Chem. Eng. Prog. 49, 88–97.
Rosa, E.S., Morales, R.E.M., 2004. Experimental and numerical development of a two-phase venturi flow meter. J. Fluids Eng. 126, 457–467.
Russell, T.W.F., Hodgson, G.W., Govier, G.W., 1959. Horizontal pipeline flow of oil and water. Can. J. Chem. Eng. 37, 9–17.
Silva, F.S., Andreussi, P., Marco, P.D., 1991. Total mass flow measurement in multiphase flow by means of a venturi meter. In: Burns, A.P. (Eds.), Presented at V. International Conference on Multiphase Production, Cannes, June 19–21, Published in Multiphase Production, Elsevier, Amsterdam, pp. 155–185.
Soubiran, J., Sherwood, J.D., 2000. Bubble motion in a potential flow within a venturi. Int. J. Multiphase Flow 26, 1771–1796.
Steven, R.N., 2002. Wet gas metering with a horizontally mounted venturi meter. Flow Meas. Instrum. 12, 361–372.
Takei, M., Ochi, M., Horii, K., Li, H., Saito, Y., 2000. Discrete wavelets auto-correlation of axial turbulence velocity in spiral single phase flow. Powder Technol. 112, 289–298.
Thang, N.T., Davis, M.R., 1979. The structure of bubbly flow through venturis. Int. J. Multiphase Flow 5, 17–37.
Thang, N.T., Davis, M.R., 1981. Pressure distribution in bubbly flow through venturis. Int. J. Multiphase Flow 7, 191–210.
Trallero, J.L., 1995. Oil–water flow patterns in horizontal pipes, Ph.D. Thesis, The University of Tulsa.
Ullmann, A., Brauner, N., 2006. Closure relations for two-fluid models for stratified smooth and stratified wavy flows. Int. J. Multiphase Flow 32, 82–105.
Valle, A., Kvandal, H., 1995. Pressure drop and dispersion characteristics of separated oil–water flow. In: Proceedings of the 1st International Symposium on Two-Phase Flow Modelling Experimentation, Rome, Italy, 9–11 October, pp. 583–591.
Vince, M.A., Lahey, R.T.J., 1982. On the development of an objective flow regime indicator. Int. J. Multiphase Flow 8, 93–124.
Wallis, G.B., 1969. One-Dimensional Two-Phase Flow. McGraw-Hill, New York.
Werven, M.V., Maanen, H.R.E.V., Ooms, G., Azzopardi, B.J., 2003. Modeling wet-gas annular/dispersed flow through a venturi. AIChE J. 49, 1383–1391.
Xu, L., Xu, J., Dong, F., Zhang, T., 2003. On fluctuation of the dynamic differential pressure signal of venturi meter for wet gas metering. Flow Meas. Instrum. 14, 211–217.
Yeh, G., Haynie Jr., F.H., Moses, R.E., 1964. Phase–volume relationship at the point of phase inversion in liquid dispersions. AIChE J. 10, 260–265.
Zhang, H.J., Yue, W.T., Huang, Z.Y., 2005. Investigation of oil–air two-phase mass flow rate measurement using venturi and void fraction sensor. J. Zhejiang Univ. Sci. 6A, 601–606.